第 27 卷第 7 期
2011 年 7 月

无 机 化 学 学 报
CHINESE JOURNAL OF INORGANIC CHEMISTRY

Vol.27 No.7
1393-1398

单晶 $CoV_2O_6·2H_2O$ 纳米带的合成及其电化学性质研究

周红洋　朱永春　钱逸泰*

(中国科学技术大学化学系,合肥微尺度物质科学国家实验室,合肥　230026)

摘要: 本文描述了在反应体系中不加入任何表面活性剂或模板的情况下,以水热法合成正交相的 $CoV_2O_6·2H_2O$ 纳米带;烧结反应得到其脱水盐,即单斜相 CoV_2O_6。通过 X 射线粉末衍射法(XRD),场发射扫描电子显微镜(FE-SEM),透射电子显微镜(TEM)和 X 射线光电子能谱(XPS)等研究了这些产物的物相、形貌和化学组成等,并通过热重分析研究了 $CoV_2O_6·2H_2O$ 纳米带的热稳定性。此外,还观察了 $CoV_2O_6·2H_2O$ 纳米带的形成过程,认为其遵循一个经典的固–液–固的形成机制。最后,通过锂离子电池实验研究了 $CoV_2O_6·2H_2O$ 纳米带及其脱水盐的电化学性质,发现其放电容量分别达到 980 和 675 $mAh·g^{-1}$。

关键词: 钒酸盐; 水热法合成; 电化学
中图分类号: O614.81+2; O614.51+1　　**文献标识码**: A　　**文章编号**: 1001-4861(2011)07-1393-06

Synthesis and Electrochemical Properties of Single-Crystalline $CoV_2O_6·2H_2O$

ZHOU Hong-Yang　ZHU Yong-Chun　QIAN Yi-Tai*

(*Department of Chemistry and Hefei National Laboratory for Physical Sciences at Microscale, University of Science and Technology of China, Hefei* 230026, *China*)

Abstract: Single-crystalline orthorhombic $CoV_2O_6·2H_2O$ nanobelts was large-scale prepared through a hydrothermal method without any templates or surfactants. The corresponding dehydrated salt of monoclinic CoV_2O_6 was prepared by the subsequent sintering treatment. The products were all collected and characterized by XRD, FESEM, TEM, SAED, HRTEM, XPS and Thermogravimetric analytical techniques. Thermogravimetric analysis indicates its thermal stability. The forming process was discussed, and we believe that the growth of nanobelts follows the typical solid-solution-solid process. Finally, the single-crystalline $CoV_2O_6·2H_2O$ nanobelts and its dehydrated salt demonstrat the first discharge of 980 $mAh·g^{-1}$ and 675 $mAh·g^{-1}$, respectively, upon electrochemical treatment in lithium ion battery.

Key words: vanadate; hydrothermal synthesis; electrochemistry

0 Introduction

In the past decades, vanadium oxides and metal vanadates attracted much attention for their special physical, chemical properties, and potential applications in the fields such as catalysts [1], chemistry sensors [2], optical devices [3], and high-energy density lithium batteries[4]. Recently, CoV_2O_6 single crystals, grown in a closed crucible, was also found to display a large magnetic anisotropy and a 1/3 magnetization plateau under a magnetic field applied along the c-axis[5].

Various efforts have been devoted to develop new approaches for the synthesis of 1D nanostructured materials. The synthesis of MnV_2O_6 was carried out through the solid state reaction between Mn_2O_3 and V_2O_5 [6]. The sintering reaction of hydrous compound

收稿日期:2010-12-10。收修改稿日期:2011-03-15。
国家 973 计划(No.2011CB935901)和国家自然科学基金(No.91022033)资助项目。
*通讯联系人。E-mail:ytqian@ustc.edu.cn

MnV_2O_6 were precipitated from the solution of $NaVO_3$ and $Mn(NO_3)_2$[7]. Stoichiometric and oxygen deficient CuV_2O_6 was prepared via co-precipitation method[8]. The hydrothermal synthetic route was also applied in synthesizing metal vanadates 1D-nanostructured single-crystal. Rod-like anhydrous crystalline powders of MnV_2O_6 were synthesized through the precipitating of mixed aqueous solution of $Mn(CH_3COO)_2$ and V_2O_5 [9]. Superlong β-$AgVO_3$ nanoribbons were synthesized from the hydrothermal reaction between V_2O_5 and $AgNO_3$ in a solution containing a small amount of pyridine [10]. $BiVO_4$ microspheres were selectively prepared through a hydrothermal process by using cetyltrimethylammonium bromide (CTAB) as a template-directing reagent [11]. $FeVO_4 0.92H_2O$ nanoneedles were fabricated via a hydrothermal method, and its electrochemical property was also investigated[12].

Previously, our group reported the synthesis of metal vanadates, i.e., Chen et al.[13] fabricated CdV_2O_6 nanowire arrays and tested its electrochemical property, Liu et al.[14], prepared single-crystal $CaV_6O_{16}\cdot 3H_2O$ and $VOx\cdot nH_2O$ nanoribbons via a hydrothermal reduction method and Liu et al.[15] synthesized $AgVO_3$ and MnV_2O_6, etc. Here we report the single-crystalline $CoV_2O_6\cdot 2H_2O$ nanobelts preparation via a hydrothermal method without introduction into the reacting system of any templates or surfactants. The dehydrated salt was also prepared from the subsequent sintering treatment. Finally, their electrochemical properties were evaluated in lithium ion battery.

1 Experimental

All the reagents used in these experiments were of analytical purity, purchased from Shanghai Chemical Reagent Company, and were used without further purification. In a typical procedure, 1 mmol $CoCl_2\cdot 6H_2O$ and 2 mmol NH_4VO_3 floccule-like white powders were put into the autoclave with 40 mL distilled water, all the solution was magnetically stirred for 15 min. Then, the autoclave was sealed, maintained at 180 ℃ for 12 h, and air cooled to room temperature. The green sponge-like product was transferred into a 100 mL beaker, filtrated, washed by distilled water and absolute ethanol at least three times. Finally, the product was dried in a vacuum at 60 ℃ for 24 h and was collected for characterization. The corresponding dehydrated salt was prepared through the subsequent treatment by sintering at 500 ℃ for 3 h in the atmosphere of argon. The product was also collected and characterized.

XRD (X-ray diffraction) patterns of the as-prepared samples were recorded using a Philips XPert PRO SUPER X-ray diffractometer equipped with graphite monochromatized Cu $K\alpha$ radiation (λ = 0.154 187 4 nm). The morphology and size of the final products were characterized by a series of microscopic techniques. Field scanning electron microscopy (FESEM) images were taken with JEOL-6700F scanning electronic microanalyzer. Transmission electron microscope (TEM) image and selected area electron diffraction (SAED) pattern were taken by Hitachi H-800 TEM with a tungsten filament and an accelerating voltage of 200 kV. High resolution transmission electron microscope (HRTEM) image was recorded on a JEOL 2010 microscope. The samples used for TEM and HRTEM characterization were dispersed in absolute ethanol and were ultrasonicated before observation. The chemical composition of the nanobelts was obtained by X-ray photoelectron spectroscopy (XPS) on a VGESCALAB MKII X-ray photoelectronic spectrometer, using non-monochromated Mg $K\alpha$ radiation as the excitation. Thermogravimetric analysis (TGA) was carried out on a TGA-50 thermal analyzer (Shimadzu Corporation) at a heating rate of 10 ℃·min^{-1} in flowing argon.

The electrode laminate for the electrochemical testing was prepared by casting a slurry consisting of $CoV_2O_6\cdot 2H_2O$ and its dehydrated salt powders(80wt %), acetylene black (10wt%), and poly (vinylidene fluoride) (PVDF; 10wt%), dispersed in 1-methyl-2-pyrrolidinone (NMP) onto a copper foil. The laminates were then dried at 70 ℃ for 1 h. The electrolyte was made with 1 mol·L^{-1} $LiPF_6$ in ethylene carbonate (EC) and diethyl carbonate (DEC; 1:1 *w/w*). Cells were then tested on a multichannel battery cycler (Shenzhen Neware Co. Ltd.)

and subjected to charge-discharge cycles at 0.30 mA·cm^{-2} between 0.005 and 3.20 V (vs. Li metal).

2 Results and discussion

The XRD pattern of the as-products is shown in Fig.1, all the peaks could be indexed as an orthorhombic phase, primitive lattice [space group: *Pnma* (No. 62)] of $CoV_2O_6\cdot 2H_2O$ with the calculated lattice constants a=0.555 nm, b=1.062 nm, c=1.191 nm, which are in good agreement with the literature results (PDF No.80-0247). No other peaks of impurity are detected. XPS analysis is employed to further confirm the element component of $CoV_2O_6\cdot 2H_2O$ nanobelts. As shown in Fig.2 (a), the survey spectra demonstrate the presence of Co, V, and O. The high-resolution XPS spectra from Co2*p* region in Fig.2(b) show the binding energies (BE) of Co2$p_{1/2}$ (797.079 eV) and Co2$p_{3/2}$ (780.774 eV), which are consistent with the literature values[16].

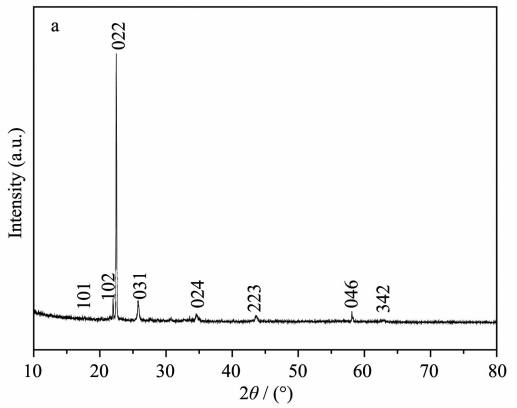

Fig.1　XRD pattern of as-prepared $CoV_2O_6\cdot 2H_2O$ sample

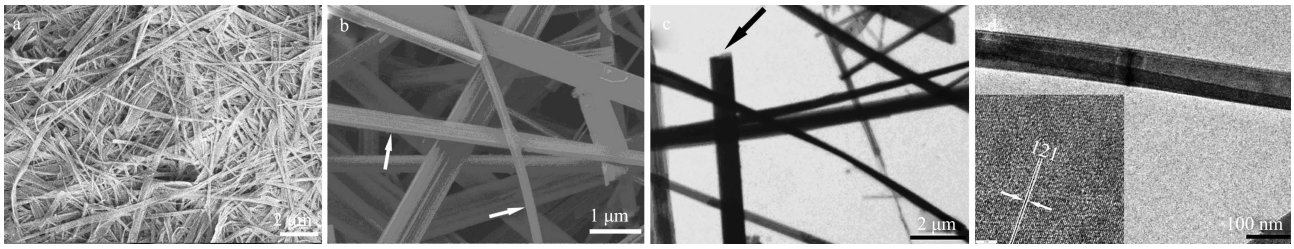

The TEM images of the as-prepared $CoV_2O_6\cdot 2H_2O$ nanobelts (c) and the single nanobelt (d) with the HRTEM image (inset)

Fig.2　low (a) and high (b) magnification FESEM image of $CoV_2O_6\cdot 2H_2O$ nanobelts

Fig.3(a) is the low magnification FESEM image of the as-prepared $CoV_2O_6\cdot 2H_2O$ single-crystal nanobelts. It shows that the product is consisted of a large quantity of nanobelts, with width of several hundreds nm, thickness of 10 nm and length up to several tens of micrometers. The twist and waving shapes of the nanoribbons are apparent. Fig.3 (b) is the high magnification FESEM image of the product. It reveals some obvious features of belt-like structure. The morphologies and microstructures were further investigated through TEM technique. Fig.3 (c) and (d) show the low magnification and high magnification TEM images of products, respectively. The TEM images indicate that the as-prepared product is uniform nanobelts in agreement with those of SEM results. As shown by the arrows in Fig.3(b) and (c), we

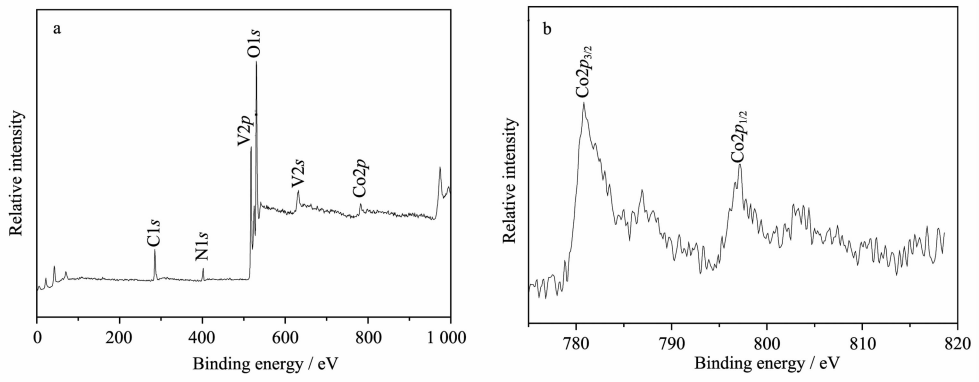

Fig.3　survey spectra (a) and high-resolution (b) XPS spectra of the as prepared $CoV_2O_6\cdot 2H_2O$ nanobelts

could observe the nanoribbons have rectangle-like cross sections. The HRTEM image of the inset in Fig. 3(d) taken from a typical nanobelt displays the clearly resolved lattice fringes, indicating the integrality of crystallinity of the nanobelt. The inter-planar spacing is 0.366 7 nm, corresponding to the (121) plane of $CoV_2O_6 \cdot 2H_2O$ orthorhombic phase. It substantiates that the nanobelts are single-crystalline ones.

Thermogravimetric analysis results further confirm the dehydrating process. As shown in Fig.4, the weight becomes constant up to 500 ℃, indicating that the dehydrating reaction happens from room temperature to 500 ℃. And the overall percentage weight loss in the thermogravimetric analysis is 11.89%, very close to the calculated value (12.30%). The corresponding sintering experiment is done as follows: the as-prepared $CoV_2O_6 \cdot 2H_2O$ nanobelts were heated from room temperature to 500 ℃ at a heating rate of 10 ℃·min^{-1} in flowing argon. After sintering for 3 h, the product was naturally cooled to room temperature, collected for characterization. As in Fig.5 (a), the XRD pattern could be indexed as a monoclinic phase, end-centered lattice [space group: *C*2 (No.5)] of CoV_2O_6 with the calculated lattice constants, a=0.924 5 nm, b=0.349 8 nm, c=0.662 2 nm, β=111.05°, which are accordant with the literature results (PDF No. 77-1174). More details of CoV_2O_6 are shown in Fig.5(b) and (c). The SEM image in Fig.5 (b) shows that the CoV_2O_6 nanocrystals comprising this pre-dehydrated product are 1D nanostructure with clear broken facets and relatively-short aspect ratio, which is possibly ascribed to the sintering treatment. The typical TEM image of a single CoV_2O_6 nanorod is also recorded, and the corresponding HRTEM image (inset) displays these clearly resolved lattice fringes with inter-planar spacings of 0.306 8 nm and 0.183 73 nm, which are corresponding to the (111) and (403) planes of the CoV_2O_6 monoclinic phase. No vacancy nor dislocation is detected among these TEM images, indicating that CoV_2O_6 nanorods are all well-crystallized under the sintering condition.

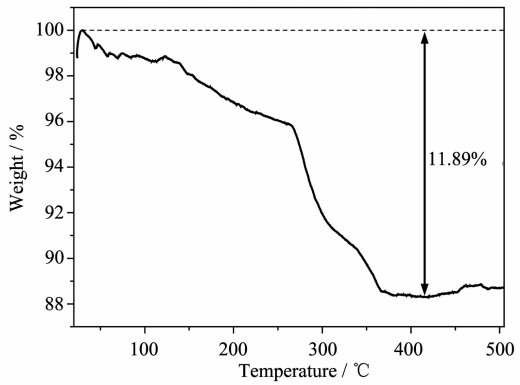

Fig.4 TGA curve of the as-prepared $CoV_2O_6 \cdot 2H_2O$ single-crystal nanobelts

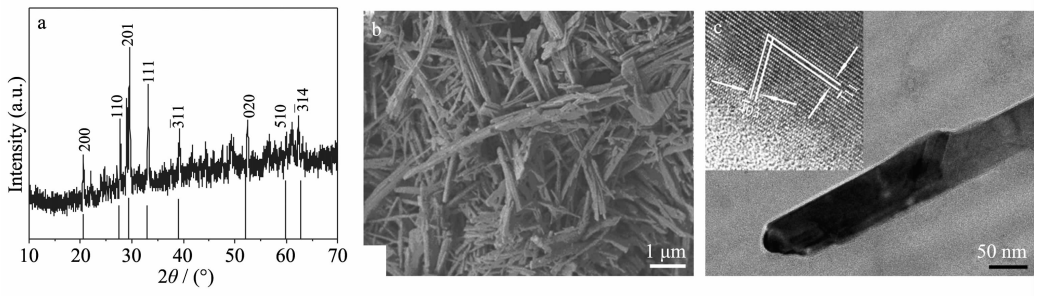

Fig.5 (a) The XRD patterns for the product prepared in sintering experiment and the literature results of the CoV_2O_6(below), the SEM image (b) for the product and the TEM image (c) of a single CoV_2O_6 nanorod with the HRTEM pattern (inset)

In order to investigate the growing process of the single-crystalline $CoV_2O_6 \cdot 2H_2O$ nanobelts, a series of time-dependent experiments were carried out, and the products of different stages at the temperature of 180 ℃: (a) 15 min. (b) 30 min. (c) 2.0 h. (d) 4.0 h., were collected and characterized. The XRD patterns shown in Fig.6 indicate that all the products could be indexed as an orthorhombic phase of $CoV_2O_6 \cdot 2H_2O$ and no other peaks are detected. The XRD result also implies that the phase of $CoV_2O_6 \cdot 2H_2O$ forms soon at the initial stage of the reacting process [as shown in Fig.6 (a) and (b), the phase forms after 30 min]. The

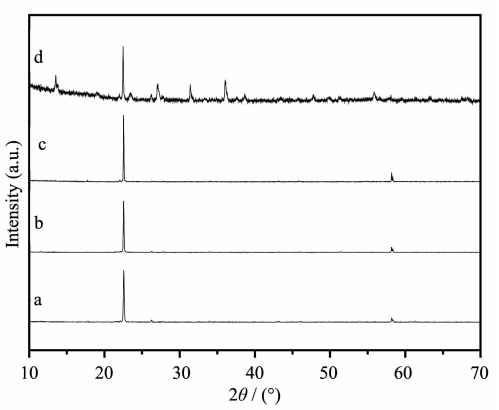

Fig.6　XRD pattern for the products synthesized by hydrothermal reaction at 180 ℃ for (a) 15 min. (b) 30 min. (c) 2.0 h. (d) 4.0 h., respectively

SEM images were also employed to observe the overall growing process. A mixture of floccules and microcrystals is formed at the initial stage (15~30 min). As shown in Fig.7 (a) and (b), these floccules include microplates with width of several micrometers and thickness of tens nanometers, the microcrystals are regular polyhedron in morphologies and tens of micrometers in size (inset). Subsequently, with the extension of reaction time, the yield of microcrystals decreases sharply. With the yield of floccules increasing, the main content of floccules is transformed into the belt-like microstructure [shown in Fig.7(c)]. When the reaction time is extended to 4.0 h, the product is almost transformed into $CoV_2O_6·2H_2O$ nanobelts without any nanocrystals of other morphology. Afterwards, the apparent morphology of the product will not change obviously by extending the reacting time. Although the exact mechanism is still unclear, we believe that the growth of nanobelts is controlled by a solid-solution-solid process (SSS), and the forming process of $CoV_2O_6·2H_2O$ single-crystal nanobelts might be described by the reaction:

$$Co^{2+}+2VO_3^-+2H_2O \rightarrow CoV_2O_6·2H_2O$$

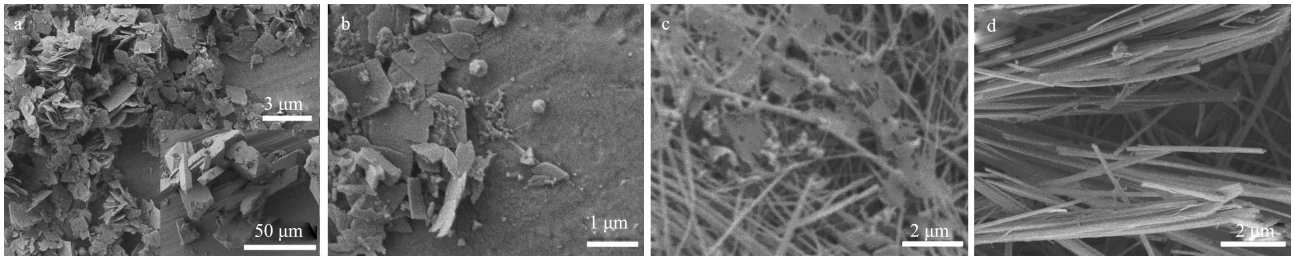

Fig.7　FESEM images for the products synthesized by hydrothermal reaction at 180 ℃ for (a) 15 min. (b) 30 min. (c) 2.0 h. (d) 4.0 h., respectively

View Within Article Previously, Baudrin et al[16] prepared a series of cobalt-based vanadates through the coprecipitation method, and investigated their electrochemical properties vs. lithium. Herein, the single-crystalline $CoV_2O_6·2H_2O$ nanobelts and their dehydrated salt were electrochemically treated in lithium ion battery to evaluate their electrochemical property. Fig.8 shows the first discharge curves of $CoV_2O_6·2H_2O$ nanobelts and its dehydrated salt at a current density of 0.3 mA·cm^{-2}. The discharge capacity of $CoV_2O_6·2H_2O$ nanobelts could reach 980 mAh·g^{-1} and its dehydrated salt can reach 675 mAh·g^{-1}. The rates of dischargeability of $CoV_2O_6·2H_2O$ nanobelts and its dehydrated salt are shown in Fig.9. After being cycled for 10 times, the capacity retention of $CoV_2O_6·2H_2O$ nanobelts is 44% (about 430 mAh·g^{-1}), and CoV_2O_6 is only 10% (about 70 mAh·g^{-1}). Investigation for the attenuation is still undergoing.

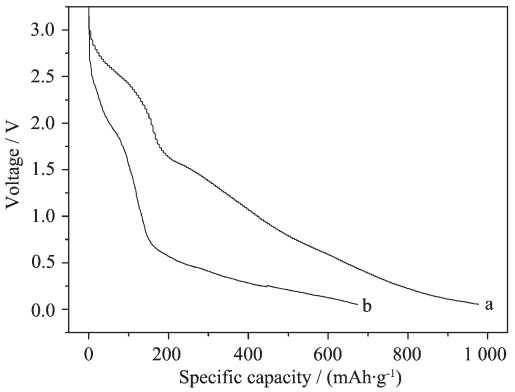

(a) $CoV_2O_6·2H_2O$ nanobelts; (b) its dehydrated salt

Fig.8　Discharge curve for the single-crystalline $CoV_2O_6·2H_2O$ nanobelts and its dehydrated salt on the first cycle

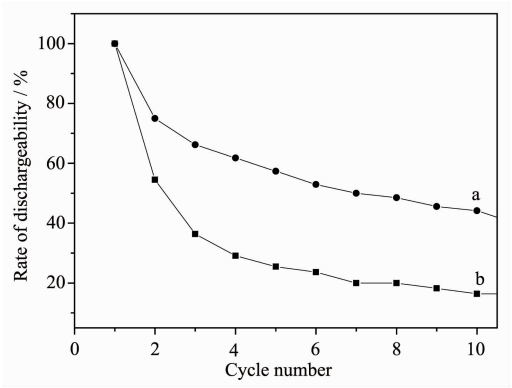

Fig.9 Rate of dischargeability of samples: $CoV_2O_6 \cdot 2H_2O$ nanobelts (a) and its dehydrated salt (b)

3 Conclusions

In summary, the single-crystalline $CoV_2O_6 \cdot 2H_2O$ nanobelts were prepared and characterized. The forming process was observed and discussed. The single-crystalline $CoV_2O_6 \cdot 2H_2O$ nanobelts and its dehydrated salts electro- chemically treated in lithium ion battery were employed to evaluate their electrochemical property, and the result suggests their potential applications in high-energy battery field.

Acknowledgment: The work was supported by the 973 Project of China (No. 2011CB935901), the National Nature Science Fund of China (No. 91022033).

References:

[1] Durand-Keklikian L. *J. Electroanal. Chem*., **2002**,**527**(1/2): 112-122

[2] Liu P, Lee S H, Cheong H M, et al. *J. Electrochem., Soc*. **2002**,**149**(3):H76-H78

[3] (a) Muster J, Kini G Y, Krsti V, et al. *Adv. Mater.*, **2000**,**12**(6):420-424

(b) Xu J F, Czerw R, Webster S, et al. *Appl. Phys. Lett.*, **2002**,**81**(9):1711-1713

[4] (a)Prosini P P, Xia Y Y, Fujieda T, et al. *Electrochimica Acta*, **2001**,**46**(17):2623-2629

(b)Prosini P P, Fujieda T, Passerini S, et al. *Electrochem. Commun.*, **2000**,**2**(1):44-47

[5] He Z Z, Yamaura J I, Ueda Y, et al. *J. Am. Chem. Soc*., **2009**, **131**(22):7554-7555

[6] Hara D, Shirakawa J, Ikuta H, et al. *J. Mater. Chem.*, **2002**, **12**(12):3717-3722

[7] (a)Piffard Y, Leroux F, Guyomard D, et al. *J. Power Sources*, **1997**,**68**(2):698-703

(b)Leroux F, Piffard Y, Ourvard G, et al. *Chem. Mater.*, **1999**, **11**(10):2948-2959

[8] Wei Y J, Nam K W, Chen G, et al. *Solid State Ionics*, **2005**, **176**(29/30): 2243-2249

[9] Inagaki M, Morishita T, Hirano M, et al. *Solid State Ionics*, **2003**,**156**(3):275-282

[10]Song J M, Lin Y Z, Yao H B, et al. *ACS Nano*, **2009**,**3**(3): 653-660

[11]Ke D N, Peng T Y, Ma L, et al. *Inorg. Chem*., **2009**,**48**(11): 4685-4691

[12]Ding N, Liu S H, Feng X Y, et al. *Cryst. Growth Des*., **2009**, **9**(4):1723-1728

[13]Chen X Y, Wang X, Wang Z H, et al. *Chem. Lett.*, **2004**,**33** (9),1160-1161

[14](a)Kong L F, Shao M W, Xie Q, et al. *J. Crystal Growth*, **2004**,**260**(3/4):435-439

(b)Kong L F, Liu Z P, Kong L F, et al. *J. Solid State Chem.*, **2004**,**177**(3):690-695

[15](a)Liu Y, Zhang Y G, Qian Y T. *Chem. Lett*., **2005**,**34**(2): 146-147

(b)Liu Y, Zhang Y G, Zhang M, et al. *J. Crystal Growth*, **2006**,**289**(1):197-201

(c)Liu Y, Zhang Y G, Du J, et al. *J. Crystal Growth*, **2006**,**291**(2):320-324

[16]WANG Jian-Qi (王建祺). *Introductory Electron Energy Spectroscopy*, Vol.1 (电子能谱学引论). Beijing: National Defense Industry Press, **1992**.

[17]Baudrin E, Laruelle S, Denis S, et al. *Solid State Ionics*, **1999**,**123**(1/2/3/4):139-153